The microbial community model MCoM 1.0: A scalable framework for modelling phototroph-heterotrophic interactions in diverse microbial communities

Leonhard Lücken[1], Michael J. Follows[2], Jason G. Bragg[3], and Sinikka T. Lennartz[1]

[1]Institute for Chemistry and Biology of the Marine Environment (ICBM), Carl von Ossietzky Universität Oldenburg, Germany
[2]Department of Earth, Atmospheric and Planetary Sciences, Massachusetts Institute of Technology, Cambridge, MA, United States
[3]Research Centre for Ecosystem Resilience, Botanic Gardens of Sydney, Sydney, New South Wales, 2000, Australia

Correspondence: Leonhard Lücken (leonhard.luecken@uol.de)

Abstract. Microbial communities, comprising phototrophic and heterotrophic microorganisms, play a crucial role in global biogeochemical cycles. However, existing biogeochemical models rarely take into account the complex interactions between these groups, usually focusing on competition for resources. In this work, we introduce the Microbial Community Model (MCoM), a framework for simulating the dynamics of diverse microbial communities. MCoM incorporates a wide range of interactions, such as cross-feeding, metabolite effects, and competition for nutrients. The model differentiates between dissolved organic nutrients (DON) and carbon (DOC), accounts for phytoplankton and heterotrophic bacterial species-specific organic matter release and uptake profiles, and simulates the impacts of bacterial metabolites on phytoplankton growth. Implemented as a box model, MCoM tracks phototrophic and heterotrophic biomass, active metabolites, DOC, DON, and inorganic nutrients through non-linear differential equations, enabling the exploration of emergent properties and feedbacks. We demonstrate the model's capabilities through simulations of experimental data of pairwise co-cultures of heterotrophic and phototrophic microorganisms, and find overall good agreement. Due to the scalable implementation, interaction matrices for larger, i.e. hundreds, of microbial groups can easily be realised. We show examples for such applications of MCoM in assessing emergent dynamics, including periodic succession patterns and multi-stability. MCoM provides a versatile, scalable, and customizable platform for assessing the range from pairwise interactions to complex microbial communities and their impact on biogeochemical fluxes.

1 Introduction

Microorganisms are the main driver of global biogeochemical cycles of major elements such as carbon, nitrogen and phosphorus. The microbially mediated turnover of these elements does not happen in isolation, because microorganisms live in diverse, interacting communities. The study of such communities in oceanic ecosystems and their adequate representation in biogeochemical models is key to understanding global elemental cycles, which in turn are crucial for the Earth's ecosystems and the habitability of the planet (Tagliabue, 2023). Arguably the two most fundamental roles in these ecosystems are primary

producers that fix inorganic carbon and nutrients into organic biomass by photosynthesis, and their counterparts, heterotrophic organisms that decompose organic matter back to CO_2 and inorganic nutrients. Biogeochemical models are powerful tools to quantify elemental fluxes mediated by these microorganisms at various scales. They can generally achieve good agreement

25   with observations in terms of common macronutrients and carbon reservoirs (e.g., Friedrichs et al., 2007; Séférian et al., 2012), and a biogeochemical component is a central part of state-of-the-art global Earth System Models.

Interactions between phototrophic and heterotrophic microorganisms are widespread, and can comprise positive and negative interactions at the same time (Cirri and Pohnert, 2019; Kost et al., 2023). On one hand, the growth rates of heterotrophic consumers are primarily driven by the availability of organic matter, which is synthesized from inorganic nutrients and carbon

30   by phytoplankton populations. A key factor influencing the composition of the heterotroph community is the specific composition of the organic material produced by phytoplankton, which varies between species (Sarmento et al., 2013; Becker et al., 2014; Mühlenbruch et al., 2018) and favors different consumers that are adapted to specific compounds (Teeling et al., 2012; Sarmento et al., 2013; Elovaara et al., 2021). Phytoplankton not only release DOM through the breakdown of previously assimilated biomass but also exude excess of newly fixed carbon (Myklestad, 2000; Thornton, 2014). The composition of these

35   exudates can vary significantly depending on environmental conditions, phytoplankton species, and growth phase, further influencing the dynamics of heterotrophic bacterial communities (Buchan et al., 2014), and the elemental ratios of this organic matter is influenced by the factor limiting their growth, resulting in varying carbon-to-nutrient ratios (Saad et al., 2016). On the other hand, phototrophs rely on the recycling of organic matter that provides new nutrients, a process mediated by heterotrophic organisms.

40   A main limitation of traditional biogeochemical modelling approaches is their focus on competition for resources among microbes, mainly phytoplankton, neglecting widespread experimental evidence that interactions between phototrophs and heterotrophs comprise positive, neutral and negative interactions resulting from cross-feeding or metabolite exchange (Sher et al., 2011; Seymour et al., 2017; Cirri and Pohnert, 2019). For example, certain bacteria release siderophores, which can either sequester iron, limiting its availability to phytoplankton or make it more accessible (Maldonado and Price, 1999; Kazamia et al.,

45   2018). Other bacteria produce algicides (Coyne et al., 2022), while some synthesize beneficial metabolites such as vitamin B12 (Sultana et al., 2023), or hormones like auxins (Amin et al., 2015). Further, heterotrophic bacteria may relieve oxidative stress on phytoplankton by degrading reactive oxygen species, e.g., hydrogen peroxide (Morris et al., 2022).

These microbial interactions are ubiquitous, and systematically affect the rates of growth and elemental turnover of microorganisms and, hence, biogeochemical fluxes (Seymour et al., 2017). Even though these interactions occur on cellular scales,

50   they may have cascading effects on the entire ecosystem with consequences for carbon cycling and, ultimately, climate regulation. However, a mathematical framework on how to incorporate these widespread microbial interactions and link it to elemental turnover is missing, hampering our ability to systematically assess their community-level effects. Existing theoretical approaches have started including cooperation (De Mazancourt and Schwartz, 2010) or facilitation (Koffel et al., 2021) into consumer-resource theory, but have not yet been applied in biogeochemical modelling. To address the middle ground between

55   purely theoretical and species specific models, we present the Microbial Community Model (MCoM), which is designed to simulate the dynamics of microbial communities, encompassing both phototrophic and heterotrophic populations and account
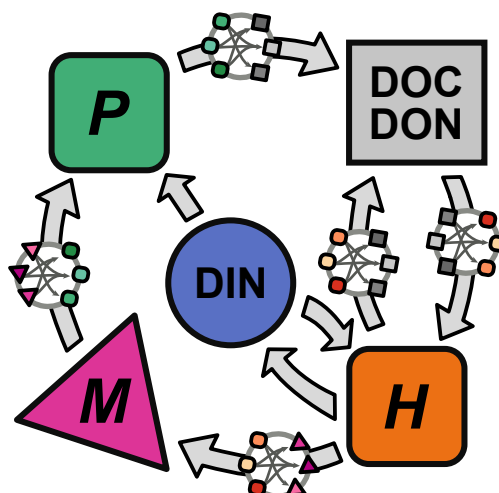
Figure 1. Model structure as flux diagram between different pools included in MCoM: phototrophic (P) and heterotrophic (H) populations, DOM (dissolved organic carbon, DOC, and nutrient, DON), metabolites (M), and inorganic nutrient (DIN). Schematic networks on links indicate complex connectivities between the components of the aggregate pools. Phytoplankton populations consume dissolved inorganic nutrients, are affected by bacterial metabolites, and release dissolved organic matter. Heterotrophic bacteria consume and release (differently composed) DOM, and consume or produce inorganic nutrient, depending on the availability of DON. Further, heterotrophs may release metabolites affecting phytoplankton growth.

for various types of interactions. MCoM incorporates features such as the differentiation of dissolved organic nutrients (DON) and carbon (DOC), DOM release profiles of phytoplankton and heterotrophic bacterial species, DOM preference profiles of heterotrophs, as well as the positive or negative impacts of bacterial products on phytoplankton growth. Additionally, the model accounts for competition for inorganic nutrients, excess production of DON and DOC by phytoplankton, and excess remineralization of DON by heterotrophic bacteria. Currently implemented as a box model, MCoM tracks state variables such as biomass, DOC, DON, and inorganic nutrients in a homogeneous volume of water through non-linear differential equations. This approach allows exploration of emergent properties and feedbacks within microbial communities, which may be essential for advancing predictive oceanic and climate modelling.

We describe the mathematical formulation and numerical implementation of the model in the Sections 2 and 3. In Section 4, we present several examples to evaluate its capabilities to fit experimental data and to describe emergent dynamics.

2 Model description

In MCoM, any momentary state of the microbial model system is represented by the following dynamic variables:

- Phytoplankton population densities $P_i(t)$, $i \in \mathcal{P}$ (cells L^{-1})

70   – Heterotroph population densities $H_i(t)$, $i \in \mathcal{H}$ (cells L^{-1})

– Concentrations of dissolved organic nutrient (DON) compounds $D_i(t)$, $i \in \mathcal{N}$ (mM(N) [$= \mathrm{mmol(N)\,m^{-3}}$])

– Concentrations of dissolved organic carbon (DOC) compounds $D_i(t)$, $i \in \mathcal{C}$ (mM(C) [$= \mathrm{mmol(C)\,m^{-3}}$])

– Concentrations of bacterial metabolites acting on phytoplankton growth $M_i(t)$, $i \in \mathcal{M}$ (L^{-1})

– The nutrient concentration $N(t)$ (mM(N))

75   We are using index sets $\mathcal{P}$, $\mathcal{H}$, $\mathcal{N}$, $\mathcal{C}$, and $\mathcal{M}$ throughout the text to enumerate the different components of a specific type. For the microbial populations, we assume fixed stoichiometric molar ratios $r_i^{C:N}$ (for $i \in \mathcal{P}$ and $i \in \mathcal{H}$) and an average cell carbon content χ_i^C. For an overview of parameters and associated physical units, we refer to Table A1. The populations are measured in cells per litre, but elemental C- and N-content can be associated unambiguously given $r_i^{C:N}$ and χ_i^C. The dynamics of a component is determined by the sum of its associated in- and outfluxes, which are denoted by f_X^Y with varying super- and

80   subscripts (*cf.* Table A2). Figure 1 summarizes these fluxes and provides a schematic overview of the model. In the following, we describe the different involved processes in detail.

2.1 Phytoplankton population dynamics

The growth of a phytoplankton population P_i is governed by

$$\frac{d}{dt}P_i = \underbrace{\left(f_{C \to i}\right.}_{\text{biomass assimilation}} \underbrace{\left. - f_{i \to \mathrm{DOC}}\right)}_{\text{biomass decay}} / \chi_i^C - \underbrace{\Delta P_i}_{\text{dispersion}}, \tag{1}$$

85   where χ_i^C is the cellular carbon content, $f_{C \to i}$ is the photosynthetic carbon assimilation flux, and $f_{i \to \mathrm{DOC}}$ summarizes losses of biomass to DOC. Assuming a fixed stoichiometric composition $r_i^{C:N}$, nutrient fluxes must fulfil

$$\underbrace{f_{C \to i} = r_i^{C:N} \cdot f_{N \to i}}_{\text{influx}}, \text{ and } \underbrace{f_{i \to \mathrm{DOC}} = r_i^{C:N} \cdot f_{i \to \mathrm{DON}}}_{\text{outflux}}. \tag{2}$$

We apply Liebig's minimum principle to distinguish two different growth regimes, depending on the limiting factor. Specifically, light intensity determines the maximal carbon assimilation rate $f_{C \to i}^{\max}$, while nutrient availability governs the maximal

90   nutrient assimilation rate $f_{N \to i}^{\max}$. As the realized fluxes must adhere to the stoichiometric constraints (2), nutrient limitation occurs when

$$r_i^{C:N} \cdot f_{N \to i}^{\max} < f_{C \to i}^{\max}, \tag{3}$$

and light limitation when $r_i^{C:N} \cdot f_{N \to i}^{\max} > f_{C \to i}^{\max}$.

2.1.1 Maximal and realized assimilation rates

95 Under conditions where nutrient availability is the primary limiting factor, nutrient uptake is defined by the nutrient concentration ($f_{N\to i} = f_{N\to i}^{\max}$) and determines phytoplankton growth. This maximal uptake is assumed to be characterized by a type-II response function:

$$f_{N\to i}^{\max} = \frac{V_{i,N} N}{K_i^N + N} P_i,\tag{4}$$

where χ_i^N is the nutrient content per cell, $V_{i,N}$ is the (theoretical) maximum nutrient uptake rate (different to $f_{N\to i}^{\max}$, which is

100 the maximal rate under current conditions) and K_i^N is the corresponding half-saturation constant. The corresponding carbon assimilation $f_{C\to i}$ is calculated according to Eq. (2).

In light-limited regimes the growth is governed by the maximal photosynthetic carbon assimilation

$$f_{C\to i}^{\max} = \phi_i(I)\,\chi_i^{\mathrm{Chl}} P_i,$$

where χ_i^{Chl} is the average chlorophyll content per cell and $\phi_i(I)$ is the P-I curve associated to phytoplankton species P_i, which

105 describes the dependence of the photosynthesis rate on the irradiance I. For the P-I curve we assume the form

$$\phi_i(I) = \phi_{s,i}\left(1 - \exp\left(\frac{-\alpha_i \cdot I}{\phi_{s,i}}\right)\right) \cdot \exp\left(\frac{-\beta_i \cdot I}{\phi_{s,i}}\right)\tag{5}$$

with initial sensitivity α_i, photoinhibition coefficient β_i and upper bound $\phi_{s,i}$ for the photosynthesis rate (Platt et al., 1980).

2.1.2 Assimilation and exudation of DOM

Phytoplankton species exude excessively fixed organic matter directly into the environment (Myklestad, 2000; Thornton, 2014).

110 In the nutrient limited regime the surplus photosynthetic capacity is assumed to be used for exudation of DOC, which is calculated as

$$f_{C\to\mathrm{DOC}}^i = f_{C\to i}^{\max} - f_{C\to i}.\tag{6}$$

In the light limited regime, exudates are assumed to be nutrient-saturated[1] and we employ an extended scheme to determine the exudation rates, because organic exudates contain a minimal amount of carbon. We assume that nutrient-rich DOM has a uniform C:N ratio $r_{\mathrm{ex},i}^{C:N}$ (with $r_{\mathrm{ex},i}^{C:N} < r_i^{C:N}$), i.e.,

$$f_{C\to\mathrm{DOC}}^i = r_{\mathrm{ex},i}^{C:N} \cdot f_{N\to\mathrm{DON}}^i.\tag{7}$$

Notably, this assumption implies that not all carbon is utilized for biomass assimilation, even though its fixation rate limits the population's growth. To maintain a balance between growth and exudation in nutrient-rich environments, we introduce a maximal fraction q_i^{ex} of $f_{C\to i}^{\max}$, up to which carbon can be allocated for exudation. A maximization of DON exudation under

---

[1]Light-limited exudation can also be switched off by setting variant.use_exudation=false.

this constraint (see Appendix B) gives

$$f_{C \to \text{DOC}}^i = \min \left(\frac{r_{\text{ex},i}^{C:N}}{r_i^{C:N} - r_{\text{ex},i}^{C:N}} \left(r_i^{C:N} f_{N \to i}^{\max} - f_{C \to i}^{\max} \right), q_i^{\max} f_{C \to i}^{\max} \right). \tag{8}$$

Figure 2 shows the resulting dependence of assimilation and exudation on nutrient availability with fixed photosynthesis rate $f_{C \to i}^{\max}$. For low nutrient concentrations, the growth rate follows the maximal nutrient uptake rate, i.e., $f_{C \to i} = r_i^{C:N} f_{N \to i}^{\max}$ (overlapping black and blue curves), *cf.* Eq. (4) and only DOC is excreted at a rate $f_{C \to DOC}^i$ (dashed gray curve). The growth

125 rate reaches its maximum around a concentration $N = 0.4\,\text{mM}$, where $r_i^{C:N} f_{N \to i}^{\max} = f_{C \to i}^{\max}$ and no DOM is excreted. For larger concentrations, the growth becomes light-limited and excreted DOM has C:N ratio $r_{\text{ex},i}^{C:N}$. Within the interval $0.4 < N < 0.47$ (shaded background), the first argument of the minimum function in Eq. (8) takes effect, and the fraction of photosynthesised organic carbon allocated to exudation is smaller than $q_i^{\max}$. For increasing nutrient an increasing share of fixed organic carbon is exuded until the share reaches the maximal value of $q_i^{\max}$ at $N \approx 0.47$ and the exudation profile becomes independent of

130 further increases in nutrient concentrations.

2.1.3 Population losses

The phytoplankton mortality is governed by the sum of three terms:

$$f_{i \to \text{DOC}} = \chi_i^C \cdot \max \left(0, \Big[\underbrace{\delta_i}_{\text{linear mortality}} + \underbrace{\delta_{q,i} P_i}_{\text{quadratic mortality}} + \underbrace{\sum_{j \in \mathcal{M}} \frac{a_{i,j} M_j}{h_{i,j} + M_j}}_{\text{metabolite production}} \Big] P_i \right), \tag{9}$$

where δ_i is the base rate of linear mortality, $\delta_{q,i}$ is the coefficient of quadratic mortality, and the sum $\sum_{j \in \mathcal{M}} \frac{a_{i,j} M_j}{h_{i,j} + M_j}$ describes

135 the total impact of present metabolites on P_i. Note that the second term in the maximum function may theoretically become negative, because the coefficients $a_{i,j}$ are allowed to be negative in order to model beneficial metabolite effects. To ensure that such a mortality reduction does not result in a positive growth, the maximum ensures the positivity of the flow $f_{i \to \text{DOC}}$.

2.2 Heterotroph population dynamics

The bacterial population densities H_i change according to:

140 $$\frac{d}{dt} H_i = \underbrace{\Big(f_{\text{DOC} \to i}}_{\text{biomass assimilation}} - \underbrace{f_{i \to \text{DOC}} \Big)}_{\text{biomass decay}} / \chi_i^C - \underbrace{\Delta H_i}_{\text{dispersion}}, \tag{10}$$

where $f_{\text{DOC} \to i}$ describes the carbon assimilation into biomass from DOC compounds and $f_{i \to \text{DOC}}$ the loss of biomass to organic compounds. As for phytoplankton, heterotrophs are modelled with a fixed stoichiometric composition $r_i^{C:N}$, which is preserved by imposing

$$\underbrace{f_{\text{DOC} \to i} = r_i^{C:N} \left(f_{\text{DON} \to i} + f_{N \to i} \right)}_{\text{influx}}, \text{ and } \underbrace{f_{i \to \text{DOC}} = r_i^{C:N} \cdot f_{i \to \text{DON}}}_{\text{outflux}}. \tag{11}$$
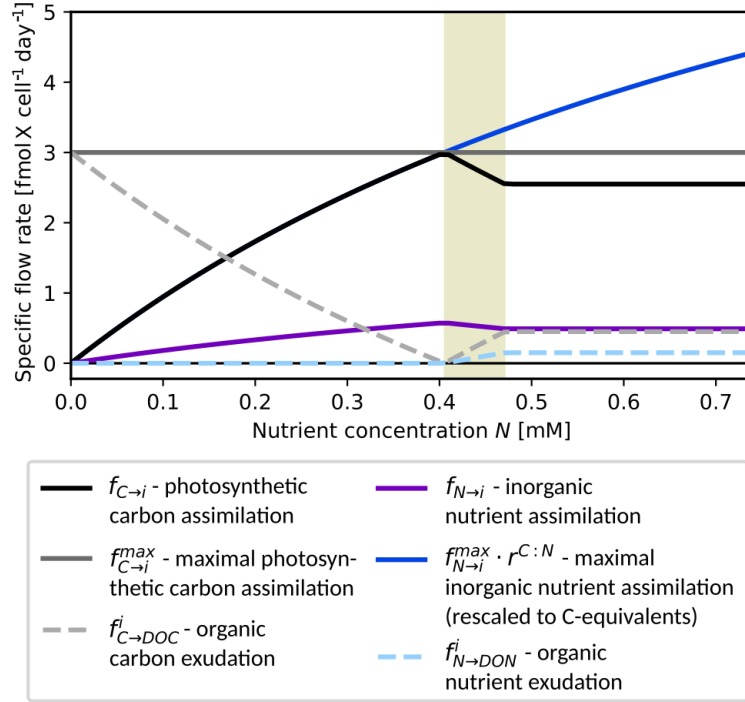
Figure 2. Excess DOM exudation by phytoplankton. Exudation rates $f_{C \to \text{DOC}}$ (gray dashed) and $f_{N \to \text{DON}}$ (light blue dashed) are plotted against nutrient availability N for a fixed photosynthesis rate $f_{C \to i}^{\max} = 3.0 \, \text{fmol(C)} \, \text{cell}^{-1} \, \text{day}^{-1}$ (dark gray) and a single cell, i.e., $P_i = 1$. Additional curves: (rescaled) maximal nutrient assimilation rate $f_{N \to i}^{\max}(N) \cdot r_i^{C:N}$ (blue), realized assimilation rates $f_{C \to i}$ (black) and $f_{N \to i}$ (purple). Other parameters for this example: $r_i^{C:N} = 5.2 \, \text{mol(C)} \, \text{mol(N)}^{-1}$, $r_{\text{ex}}^{C:N} = 3.0 \, \text{mol(C)} \, \text{mol(N)}^{-1}$, $q_i^{\max} = 0.15$, $V_{i,N} = 2.0 \, \text{day}^{-1}$, $K_i^N = 1.0 \, \text{mM(N)}$.

145   Since heterotrophic populations are assumed to obtain nutrients from inorganic and organic sources, the constraint for the influx involves both sources. Importantly, the DOM assimilation fluxes are aggregates of fluxes from individual compounds, i.e.,

$$f_{\text{DOC} \to i} = \sum_{j \in \mathcal{C}} f_{j \to i}, \text{ and } f_{\text{DON} \to i} = \sum_{j \in \mathcal{N}} f_{j \to i}. \tag{12}$$

Growth may be limited either by DOC or by total (organic and inorganic) nutrient availability, and the realized assimilation

150   flux is determined by a minimum principle comparing maximal total assimilation rates of carbon ($f_{\text{DOC} \to i}^{\max}$) and nutrient ($f_{N \to i}^{\max} + f_{\text{DON} \to i}^{\max}$). A population H_i is nutrient limited if

$$r_i^{C:N} \left(f_{N \to i}^{\max} + f_{\text{DON} \to i}^{\max} \right) < f_{\text{DOC} \to i}^{\max}, \tag{13}$$

and energy limited if the opposite holds.

2.2.1 Maximal assimilation rates

The maximal uptake rate of an individual organic compound D_j by population H_i is modelled as

$$f_{j \to i}^{\text{up,max}} = \frac{V_{i,j} D_j}{K_{i,j} + D_j} H_i, \text{ for } j \in \mathcal{N} \text{ or } j \in \mathcal{C}. \tag{14}$$

Here, $V_{i,j}$ is the (theoretical) maximal uptake rate [*cf.* Eq (4)] and $K_{i,j}$ is the corresponding half-saturation constant. Similarly, the maximal uptake of inorganic nutrient is

$$f_{N \to i}^{\max} = \frac{V_{i,N} N}{K_i + N} H_i. \tag{15}$$

When consuming DOM compounds, a part of the compounds is assumed to be catabolized, i.e., metabolically degraded for energy extraction. Hence, only a part of the uptake is available for integration into biomass and the remainder is remineralized and released into the inorganic nutrient and carbon pools. Correspondingly, the maximal assimilation rate for the compound D_j is calculated as

$$f_{j \to i}^{\max} = Y_{i,j} f_{j \to i}^{\text{up,max}}, \tag{16}$$

where the yield coefficient $Y_{i,j}$ determines the assimilated fraction. The resulting maximal organic assimilation fluxes are

$$f_{\text{DOC} \to i}^{\max} = \sum_{j \in \mathcal{C}} Y_{i,j} f_{j \to i}^{\text{up,max}}, \text{ and, } f_{\text{DON} \to i}^{\max} = \sum_{j \in \mathcal{N}} Y_{i,j} f_{j \to i}^{\text{up,max}}. \tag{17}$$

2.2.2 DOM assimilation and remineralization

If the population H_i grows under nutrient limited conditions, it takes up and assimilates DON compounds at the maximum possible rates, i.e.,

$$f_{j \to i} = Y_{i,j} f_{j \to i}^{\text{up,max}}, \text{ for } j \in \mathcal{N}. \tag{18}$$

The fraction of DON uptake, which is not assimilated, is remineralized and induces a flow from the organic pool D_j to the inorganic nutrient pool N:

$$f_{j \to N}^{i} = (1 - Y_{i,j}) f_{j \to i}^{\text{up,max}}. \tag{19}$$

Further, the inorganic nutrient is assimilated at maximum rate $f_{N \to i} = f_{N \to i}^{\max}$ as well. Adhering to the stoichiometric constraints (11), the uptake of DOC is regulated down. We assume that this regulation decreases the uptake of all available DOC compounds proportionally, i.e., for $j \in \mathcal{C}$, $f_{j \to i}^{\text{up}} = c \cdot f_{j \to i}^{\text{up,max}}$ with a factor $c = r_i^{C:N} \left(f_{N \to i}^{\max} + f_{\text{DON} \to i}^{\max} \right) / f_{\text{DOC} \to i}^{\max}$, yielding corresponding assimilation and remineralization fluxes of

$$f_{j \to i} = Y_{i,j} f_{j \to i}^{\text{up}}, \text{ and } f_{j \to C}^{i} = (1 - Y_{i,j}) f_{j \to i}^{\text{up}}. \tag{20}$$

In carbon limited situations [Eq. (3) is not fulfilled], DOC is used at maximum rates, i.e., for all $j \in \mathcal{C}$:

$$f_{j \to i}^{\text{up}} = f_{j \to i}^{\text{up,max}}, \text{ and } f_{j \to i} = Y_{i,j} f_{j \to i}^{\text{up,max}}. \tag{21}$$

While the total assimilation rate of nutrient is tied to $f_{\mathrm{DOC}\to i}$ by stoichiometry, MCoM implements two variants of how heterotrophs behave with regard to excess DON uptake capacities.[2] Either, (i) heterotrophs still take up maximal amounts of DON and eventually remineralize any excess, or (ii) they homogeneously decrease the uptake rates for the different DON compounds such that nutrient assimilation matches carbon assimilation. The latter regulation is implemented analogously as above for DOC compounds in the nutrient limited case. In any case, we assume that DON is used preferentially and inorganic nutrient is only taken up to a degree necessary to serve the nutrient demands. More explicitly, for variant (i) we assume that $f^{\mathrm{up}}_{j\to i} = f^{\mathrm{up,max}}_{j\to i}$ for $j \in \mathcal{N}$. If the DON uptake exceeds DOC uptake, i.e.,

$$r^{C:N}_i f^{\max}_{\mathrm{DON}\to i} > f^{\max}_{\mathrm{DOC}\to i}, \tag{22}$$

additional remineralization occurs:

$$f^{+}_{\mathrm{DON}\to N} = f^{\max}_{\mathrm{DON}\to i} - f^{\max}_{\mathrm{DOC}\to i}/r^{C:N}_i. \tag{23}$$

If Eq. (22) holds for variant (ii), the realized uptake rates for DON compounds are modified as $f^{\mathrm{up}}_{j\to i} = c \cdot f^{\mathrm{up,max}}_{j\to i}$ with a factor $c = f^{\max}_{\mathrm{DOC}\to i} / \left(r^{C:N}_i f^{\max}_{\mathrm{DON}\to i} \right)$ and $f^{+}_{\mathrm{DON}\to N} = 0$.

Figure 3 shows the uptake, remineralization, as well as assimilation for varying DON at fixed DOC and inorganic nutrient concentrations. For growth limiting concentrations of DON, DON availability controls the population growth rate and is remineralized at a minimal fraction. For intermediate concentrations, the fraction of remineralized DON remains the same but less and less inorganic nutrient is used (shaded interval $0.33 < \mathrm{DON} < 0.47$) . For DON concentrations above $0.47\,\mathrm{mM}$, all nutrient requirements are served by DON and for increasing concentrations, the surplus DON is completely remineralized [variant (i), solid light blue curve] or DON remineralization rates remain constant for higher DON concentrations [variant (ii), dashed light blue curve].

2.2.3 Population loss and metabolite investment

Heterotroph biomass loss is assumed to consist of three components:

$$f_{i\to\mathrm{DOC}} = \chi^C_i \cdot \left(\underbrace{\delta_i H_i}_{\text{linear mortality}} + \underbrace{\delta_{q,i} H^2_i}_{\text{quadratic mortality}} \right) + \underbrace{\Pi_i.}_{\text{metabolite production}} \tag{24}$$

Here, δ_i is the base rate of linear mortality, $\delta_{q,i}$ is the quadratic mortality coefficient, and

$$\Pi_i = \sum_{j\in\mathcal{M}} \pi_{j,i} f_{\mathrm{DOC}\to i} \tag{25}$$

is the metabolite production investment with fractions $\pi_{j,i}$ of newly assimilated biomass expended for the production of metabolite M_j.

---

[2]This behaviour is controlled by the parameter variant.surplus_remineralization.
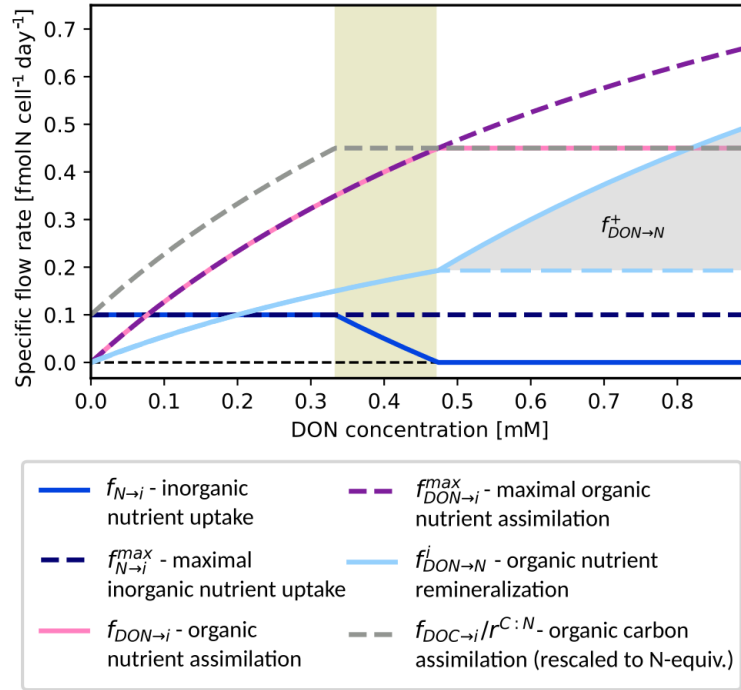
Figure 3. Bacterial remineralization of DON by one cell of a population H_i. Remineralization rate $f^i_{\text{DON} \to N}$ (light blue) plotted against DON availability at constant nutrient and DOC concentrations. Variants with (solid) and without (dashed) differ for DON levels ($> 0.47\,\text{mM}$). Additional curves: assimilation of DOC (rescaled), DON and DIN $f_{\text{DOC} \to i}/r^{C:N}_i$, $f_{\text{DON} \to i}$, and $f_{N \to i}$, maximal nutrient and DON assimilation $f^{\max}_{N \to i}$ and $f^{\max}_{\text{DON} \to i}$, and remineralization $f^i_{\text{DON} \to N}$. Parameters for this example: $r^{C:N}_i = 0.4$, $V_{i,\text{DON}} = 2.0$, $K_{i,\text{DON}} = 1.0$, $Y_{i,\text{DON}} = 0.7$. Maximal nutrient and carbon assimilation rates: $f^{\max}_{N \to i} = 0.1$ and $f^{\max}_{\text{DOC} \to i} = 1.8$.

2.3 DOM dynamics

The dynamics of individual DOM compounds are considered to follow the form

$$\frac{d}{dt} D_j = f_{H \to j} + f_{P \to j} + f_{C \to j} - f_{j \to H} - f_{j \to C} - \Delta D_j, \ \text{ for } j \in \mathcal{C}, \tag{26a}$$

$$\frac{d}{dt} D_j = \underbrace{f_{H \to j} + f_{P \to j}}_{\text{population decay}} + \underbrace{f_{N \to j}}_{\text{exudation}} - \underbrace{f_{j \to H} - f_{j \to N}}_{\text{uptake}} - \underbrace{\Delta D_j}_{\text{dispersion}}, \ \text{ for } j \in \mathcal{N}. \tag{26b}$$

Here, influxes originate from phytoplankton and heterotroph population decay and from DOM exudation by phytoplankton, and outfluxes correspond to consumption by heterotrophs.

In Secs. 2.1 and 2.2, we introduced the aggregate fluxes $f_{i \to \mathrm{DOC}}$ and $f_{i \to \mathrm{DON}}$, $i \in \mathcal{P}$ or $i \in \mathcal{H}$. To determine their impact on

215 the concentrations on individual DOM compounds D_j, we assume specific partitioning coefficients

$$\sum_{j \in \mathcal{C}} \mathrm{R}_{j,i} = \sum_{j \in \mathcal{N}} \mathrm{R}_{j,i} = 1. \tag{27}$$

That is, the individual fluxes are calculated as

$$f_{i \to j} = \mathrm{R}_{j,i} f_{i \to \mathrm{DOC}}, \text{ for } j \in \mathcal{C}, \tag{28a}$$

$$f_{i \to j} = \mathrm{R}_{j,i} f_{i \to \mathrm{DON}}, \text{ for } j \in \mathcal{N}. \tag{28b}$$

220

For simplicity, the excess DOC- or DON-exudation $f^i_{C \to \mathrm{DOC}}$ and $f^i_{N \to \mathrm{DON}}$ by phytoplankton is assumed to follow the same partitioning to individual compounds:

$$f^i_{C \to j} = \mathrm{R}_{j,i} f^i_{C \to \mathrm{DOC}}, \text{ for } j \in \mathcal{C}, \tag{29a}$$

$$f^i_{N \to j} = \mathrm{R}_{j,i} f^i_{N \to \mathrm{DON}}, \text{ for } j \in \mathcal{N}. \tag{29b}$$

225

Further, we denote the total uptake and remineralization fluxes per compound by

$$f_{j \to N} = \sum_{i \in \mathcal{H}} f^i_{j \to N}, \ f_{j \to C} = \sum_{i \in \mathcal{H}} f^i_{j \to C}, \ f_{j \to H} = \sum_{i \in \mathcal{H}} f_{j \to i}. \tag{30}$$

2.4 Metabolite dynamics

Metabolite pools M_j are modelled without any specific stoichiometry, since their contribution to the total DOM is assumed to

230 be negligible. The energy expenditure for their synthesis is modelled by the corresponding loss term in Eq. (24). The pseudo-concentrations M_j represent a basis to calculate the impact of metabolite M_j on susceptible phytoplankton species as described in Sec. 2.1. They are governed by production and decay:

$$\frac{d}{dt} M_j = \underbrace{\theta_j \sum_{i \in \mathcal{H}} \pi_{j,i} f_{\mathrm{DOC} \to i}}_{\text{production}} - \underbrace{\delta_j M_j}_{\text{decay}} - \underbrace{\Delta M_j}_{\text{dispersion}} . \tag{31}$$

Here, the coefficient θ_j determines the amount of biomass required to synthesize a unit of M_j and δ_j determines the decay rate

235 of M_j.

2.5 Nutrient dynamics

The change of nutrient concentration is driven by uptake from phytoplankton and heterotrophs and remineralization of DON by heterotrophs. Further, MCoM permits to define an external nutrient concentration N_{ext} to model a diffusive exchange with

an external domain:

$$\frac{d}{dt}N = \underbrace{f_{\mathrm{DON}\to N}}_{\text{remineralization}} - \underbrace{(f_{N\to P} + f_{N\to H})}_{\text{consumption}} - \underbrace{\Delta\,(N - N_{\mathrm{ext}})}_{\text{dispersion}}. \tag{32}$$

Here, the aggregate flows are defined as

$$f_{\mathrm{DON}\to N} = \sum_{i\in\mathcal{H}}\sum_{j\in\mathcal{N}} f^i_{j\to N}, \; f_{N\to P} = \sum_{i\in\mathcal{P}} f_{N\to i}, \text{ and } f_{N\to H} = \sum_{i\in\mathcal{H}} f_{N\to i}. \tag{33}$$

2.6 Scaling up to diverse microbial communities

A key feature of MCoM is the straightforward scalability to larger interaction networks. The size and connectivity of the interaction network, i.e., the number of phototroph populations, heterotroph populations, metabolites, and organic compounds can be specified in the configuration file, together with respective parameter values and interaction matrices. MCoM offers different built-in ways to define microbial communities and their interaction networks: For controlled set-ups, it is possible to define all rates and interactions explicitly. This explicit definition allows the user to write their own algorithms for the generation of the community's interaction network. To generate randomized networks, the entire community or a subset of parameters can be determined stochastically. When employing stochastic network generation, reproducibility can be ensured by setting a seed for the random generation.[3] For instance, the user can quickly set up a community by providing the number of phototrophs, heterotrophs, resources and metabolites, specifying the in- and output of populations (the number of produced resources and metabolites, as well as the number of consumed resources in case of heterotrophs and the number of metabolites affecting the population in case of phototrophs) and value ranges for the other system parameters. A specific option[4] allows to define a community of phototroph-heterotroph pairs, which only interact by exchange of DOM and metabolites within the pairs, i.e., all adjacency matrices are diagonal. Additional functions to generate interaction matrices according to customized requirements can easily be implemented.

## 3 Implementation and performance

3.1 Integration scheme

Starting from a given initial state $\boldsymbol{X}_0 = (\boldsymbol{P}_0, \boldsymbol{H}_0, \boldsymbol{D}_0, \boldsymbol{M}_0, N_0)$, MCoM generates trajectories using an Adams-Bashforth explicit two-step method (Butcher, 2005). This method generates state approximations at equidistant time points $t_n = t_0 + n\cdot dt$ using the formula

$$\boldsymbol{X}_{n+2} = \boldsymbol{X}_{n+1} + \left[\frac{3}{2}f\left(t_{n+1}, \boldsymbol{X}_{n+1}\right) - \frac{1}{2}f\left(t_n, \boldsymbol{X}_n\right)\right] dt, \tag{34}$$

where $\boldsymbol{X}_n$ is the vector containing the system state at time t_n. As any method, this can lead to inaccuracies when using larger time steps. In case that a solution seems to show numerical artifacts it advisable to compare the behaviour to a solution obtained with smaller step width.

---

[3]Parameter run.system_seed

[4]Parameter variant.competing_pairs
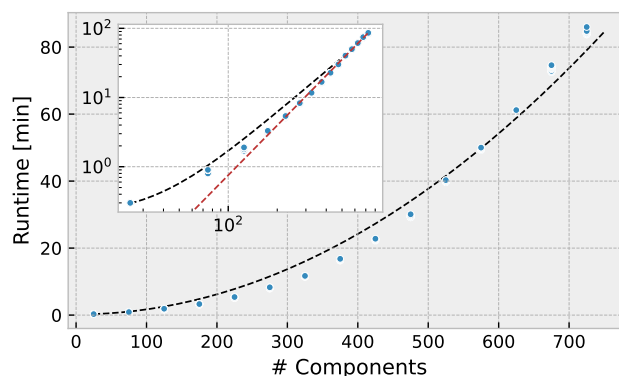
Figure 4. Computation time (wall time) for varying total network size. The total number of components is the sum of the numbers of different P_i, H_i, D_i, and M_i. For each size 16 different random communities were simulated for 100 years. Inset shows the same data in a log-log plot and a red dashed line with slope $\gamma = 2.4$.

3.2 Performance

MCoM is suited to simulate large communities comprising diverse species, DOM compounds, and metabolites. However, the numerical complexity and memory requirements of the simulation rise with system size. We assessed the performance of
270 MCoM in a simple test recording run times for different system sizes. The results are shown in Figure 4. For each number $n \in \{5, 10, ..., 150\}$, we initialized 16 random networks with n components of each type (heterotrophs, phototrophs, DOC, DON, and metabolites) and 30% connectivity. That is, for $n = 30$, each phototroph population produces 10 different DOC and 10 different DON compounds and is affected by 10 metabolites. Each heterotroph population produces the same variety of DOM compounds, is able to consume 10 DOC and 10 DON types, and produces 10 different metabolites. We simulated each
275 community for 100 years with an integration step width of $dt = 0.025$ days, saving the last ten years of the simulation to disc saving the system's state every $dt_{\text{out}} = 0.5$ days. Asymptotically, the computation time scales as n^γ with exponent $\gamma = 2.4$, as determined by the asymptotic slope of the graph of $\log n$ versus logarithmic computation time (dashed red line in the inset of Fig. 4). The black dashed curve shows a quadratic polynomial fit to the computation time.

4 Evaluation and application

280 ### 4.1 Evaluation of network motifs without metabolite-induced feedbacks: Nutrient Remineralization in *Synechococcus* co-cultures

Here, we are evaluating model performance for individual motifs of the interaction network as the smallest unit in diverse microbial communities. In a first example, we apply the simplest version of the model, i.e., a co-culture of one phototrophic and one heterotrophic strain, without any metabolite-induced feedbacks, to an incubation experiment to assess its capability
285 to reproduce the observed temporal variation in cell abundances. Christie-Oleza et al. (2017) cultured *Synechococcus* popu-
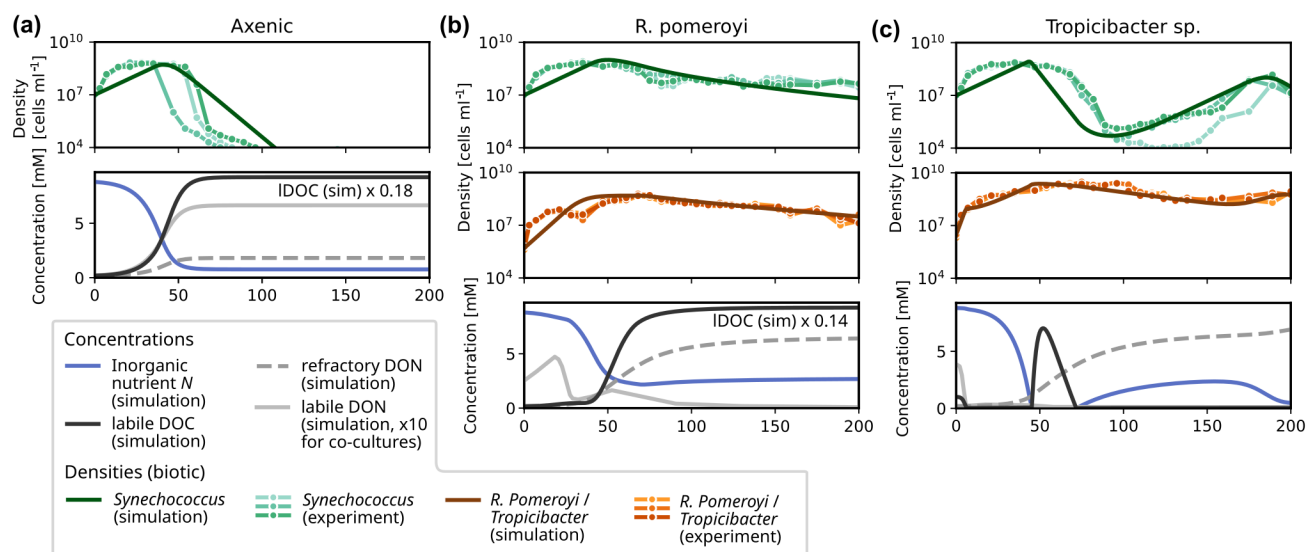
Figure 5. Experimentally observed and modelled growth dynamics of *Synechococcus* in co-culture with different heterotrophic bacteria: (a) axenic culture; (b) co-culture with *R. Pomeroyi*; (c) co-culture with *Tropicibacter sp.* For each experimental setup, three replicates were prepared, which are shown in the upper plot of each panel, see (Christie-Oleza et al., 2017) for details. For the simulations, we report *Synechococcus* (dark green) and heterotroph densities (brown), and concentrations of inorganic nutrient (blue), of labile DOC (black), labile DON (solid gray) and refractory DON (dashed gray).

lations over a 200-day period in co-cultures with two different heterotrophic bacteria (*R. Pomeroyi* and *Tropicibacter sp.*) in nutrient enriched ASW medium. When grown axenically, the phototroph population went extinct around day 75–100. If it was co-cultured with a heterotroph, it remained active until the end of the experiment at day 200. The decisive interaction was hypothesized to be an exchange of organic material, which provided the heterotrophs with energy and organically bound nutrient, and of remineralized nutrient, which could be assimilated by *Synechococcus*. Although the phototroph population densities reached a peak around days 30–40 for each setup, they showed significantly distinct growth trajectories for the different types of heterotrophs. When grown together with *R. Pomeroyi*, the subsequent population decay proceeded steadily at a relatively slow rate until reaching $2.7 - 4.4 \times 10^7 \, \text{cells ml}^{-1}$ at day 200. For *Tropicibacter sp.*, the temporal development after the initial peak is less stable (*cf*. Fig. 5c). Within the subsequent 60–70 days, *Synechococcus* collapsed to minima of $1.0 - 13.0 \times 10^5 \, \text{cells ml}^{-1}$ attained around days 96–117 for this case. These minima were then followed by a gradual recovery of until reaching another peak at density $3.6 - 14.7 \times 10^7 \, \text{cells ml}^{-1}$ at the penultimate measurement time around day 190, declining again at the last measurement on day 200 to densities $1.1 - 2.1 \times 10^7 \, \text{cells ml}^{-1}$.

We modelled both co-cultures and the axenic growth using MCoM with fixed growth parameters for the phototroph and specific characteristics for the heterotrophs. The exact parameters are listed in Table C1. Importantly, we did not assume metabolite interactions, but the observations could be reproduced qualitatively by the exchange of nutrients in inorganic and organic form.

14

As an important characteristic of *R. Pomeroyi*, we incorporated the observation that it did not use the inorganic nutrient [as demonstrated in another experiment of Christie-Oleza et al. (2017)]. Further, we assumed that *R. Pomeroyi* immediately remineralizes 30% of DON during uptake, thus providing a steady nutrient source for *Synechococcus*. The simulation showed that the recycling of nutrients slowed down population decline significantly. However, to reproduce the steady decline observed in the experiment, a certain fraction of nutrients must continuously escape the recycling. Otherwise, the total nutrient in both populations and thus their densities would asymptote towards positive constants. We incorporated this by assuming that a fraction (10% for *R. Pomeroyi*) of the DON release is channelled into a refractory pool, which accumulates during the experiment.

For *Tropicibacter sp.*, we hypothesized that the more severe collapse of the *Synechococcus* population was partly caused by an ongoing competition for inorganic nutrient with *Tropicibacter sp.*, which is assumed to be a strong competitor (smaller K_N than *Synechococcus*). Further, we modelled *Tropicibacter sp.* to behave more parsimoniously releasing only 5% of the DON it takes up in inorganic form. This assumption leads to a domination of the heterotroph until DOC is depleted and it becomes energy-limited, making inorganic nutrient available for *Synechococcus* once again and leading to the observed smaller second peak. Notably, the fit was significantly improved by assuming a more efficient and complete utilization of *Synechococcus* exudates by *Tropicibacter sp.* in comparison to *R. Pomeroyi*.

4.2 Evaluation of network motifs with metabolite-induced feedbacks: Interactions in *Prochlorococcus* co-cultures

In a next step, we evaluate MCoM's ability to model metabolite-induced feedbacks between heterotrophs and phototrophs. For this, we consider co-culture experiments of *Prochlorococcus* and different heterotrophic bacteria conducted by Sher et al. (2011), which were initially supplied with a stock of $0.8\,\mathrm{mM}\,\mathrm{NH}_4$. In comparison to axenic cultures [Fig. 6(a)], Sher et al. observed different possible outcomes for different heterotrophic bacteria. Based on the cultures' observed bulk chlorophyll fluorescence over time, they clustered the heterotrophs into clearly separated groups exhibiting either inhibitory, neutral or growth-promoting effects on *Prochlorococcus* growth. Growth-promoting bacteria induced an earlier (-4 days on average) and more pronounced peak of the phototroph population than observed for the axenic (or neutrally affected) cases, while inhibitory bacteria significantly delayed the peak ($+13$ days on average).

We chose two representative examples from the experimental arrays published by Sher et al. (2011) for illustration. In co-culture with a *Rhodobacterales* strain (HOT5B8), Prochlorococcus growth was clearly promoted [Fig. 6(b)], whereas in co-culture with a *Marinobacter* strain (HOT4B5), growth was inhibited [Fig. 6(c)]. For the simulations, we used identical parameters for both heterotrophs and only varied the metabolite impact coefficient a_M [*cf.* Eq. (9), simplified subscript] using $a_M = -0.2$ for the growth promoting case and $a_M = 0.17$ for the inhibitory case.

For both modelled co-cultures the simulated metabolite concentrations initially accumulate leading to a saturation at full effect strength around day 10 (purple curves in Fig. 6). For the growth-promoting case, metabolite effects decrease the loss rate of the *Prochlorococcus* population. Thereby the net growth rate of phototrophs is increased, leading to larger populations and accelerated depletion of the inorganic nutrient when compared to the axenic culture. For the inhibitory case, metabolite effects reduce the phytoplankton net growth rate. For both co-cultures, simulated DOC (black curves in Fig. 6) accumulates in the first days because the initial heterotrophic densities are low. This accumulation is less pronounced for the growth-
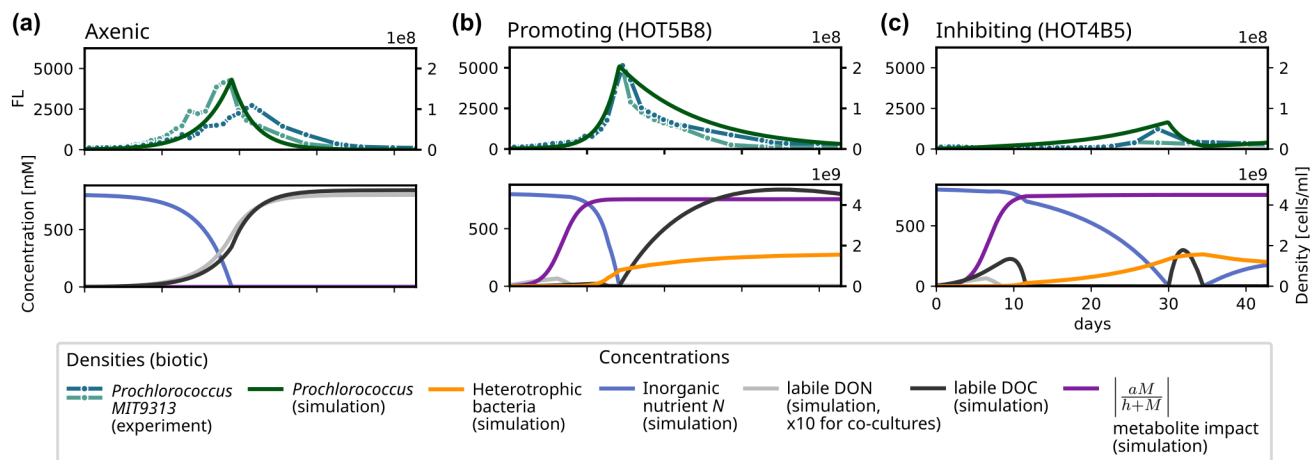
Figure 6. Experimentally observed and modelled growth dynamics of *Prochlorococcus* (MIT9313) in co-culture with different heterotrophic bacteria (Sher et al., 2011): (a) axenic culture; (b) co-culture with *Rhodobacterales* strain (HOT5B8); (c) co-culture with *Marinobacter* strain (HOT4B5). For each experimental setup, two replicates were prepared, which are shown in the upper plot of each panel. The simulated *Prochlorococcus* density (dark green curve) is plotted on top of the bulk chlorophyll fluorescence observed in the experiments. For the simulations, we report *Prochlorococcus* and heterotroph densities, P and H, and concentrations of inorganic nutrient (N, blue), of labile DOC (black), and labile DON (solid gray). Further, we show the impact strength $\left|\frac{aM}{h+M}\right|$ of metabolites M on the mortality rate of P (solid purple). The model parameters used in this section are listed in Table C2.

promoting case due to the lower *Prochlorococcus* mortality. Around day 12 the accumulated DOC is depleted to minimal levels and heterotrophic growth becomes directly locked to DOC-release by phytoplankton. The DOC-locked regime lasts until the depletion of the inorganic nutrient stock, which coincides with the *Prochlorococcus* population peak. This happens at day 14 for the growth-promoting case, at day 19 for the axenic culture, and at day 30 for the inhibitory case. These differences

340   are caused by the different phytoplankton growth rates in the different scenarios, which largely determine the consumption rate of inorganic nutrient. After this point DOC starts to accumulate again, since heterotrophic growth becomes nutrient-limited. For the inhibitory case, this second phase of DOC accumulation is less pronounced due to the lower phytoplankton densities. Rather, we observe a second depletion of DOC at day 34 of the simulated experiment. This depletion is followed by a phase, where nutrient concentrations rise due to heterotrophic remineralization of surplus DON, comparable to the hypothesized

345   succession of events for the co-culture of *Synechococcus* and *Tropicibacter sp.* [Fig. 5(c)]. In conclusion, with a variation of single parameter (a_M) MCoM can capture both, the temporal shifts of the population peaks and the changes of the maximal observed *Prochlorococcus* density.
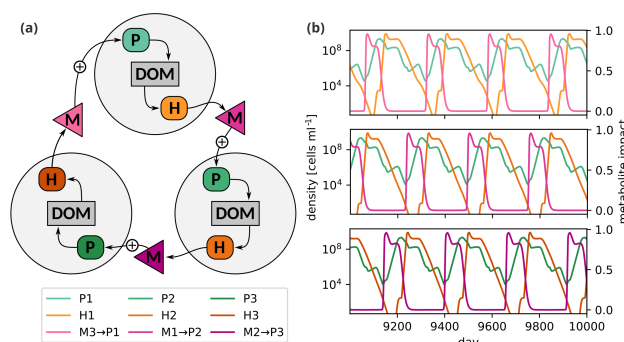
Figure 7. (a) Cyclic interaction scheme of three consortia; (b) Simulated population densities and metabolite impacts. The data of a single simulation is distributed over three panels to avoid cluttering of curves. See Table C3 for parameters.

4.3 Application for studying phytoplankton succession: Metabolite interactions lead to fluctuating dynamics

Having evaluated MCoMs ability to reproduce dynamics of individual motifs, which may represent components in a larger
350 microbial interaction network, we now show two examples of MCoM's application when scaled up to more diverse microbial
communities. First, we consider a cyclic interaction network to illustrate how feedbacks mediated by metabolite interactions
can lead to self-sustained fluctuations in a community of three phytoplankton and three heterotroph populations [Fig 7(a)]. We
model associations of specific heterotroph and phytoplankton species, H_i and P_i, by stipulating that the heterotroph H_i spe-
cializes on the consumption of organic matter produced by the phototroph P_i, forming a "consortium". Due to this syntrophic
355 relationship population peaks of P_i tend to be succeeded by peaks of H_i. Further, different consortia are assumed to be coupled
via metabolites, such that metabolites produced by H_i positively affect P_{i+1}. Effectively, this causes population peaks of H_i
to be succeeded by peaks of P_{i+1}, and so on, leading to a "merry-go-round" succession of consortia. Figure 7(b) shows the
corresponding trajectory from day 9000 to 10000 after it has settled on a periodic orbit. While such a setup may appear highly
artificial, it is robust to parameter variations and illustrates the potential of metabolite feedbacks to incite non-stationarity of
360 population densities even if no environmental forcing is present.[5]

4.4 Application for studying community stability: Metabolite interactions facilitate priority effects in microbial consortia

Generalizing the notion of a "consortium" as a coherent sub-community, we randomly generated communities consisting of
separate highly connected groups of species. A consortium in this sense can loosely be defined as a set of phototrophs, DOM
365 compounds, heterotrophs and metabolites, which interact mostly within themselves. That is, within a consortium, heterotrophs
feed on DOM released by members of the consortium, and phototroph growth is positively affected by metabolites produced by

---

[5]In natural situations, successions are regularly reported as a response to an initial environmental impulse, such as seasonal upwelling of nutrients. These scenarios can also be modelled with MCoM specifying a fluctuation for the parameter environment.nutrient.

17
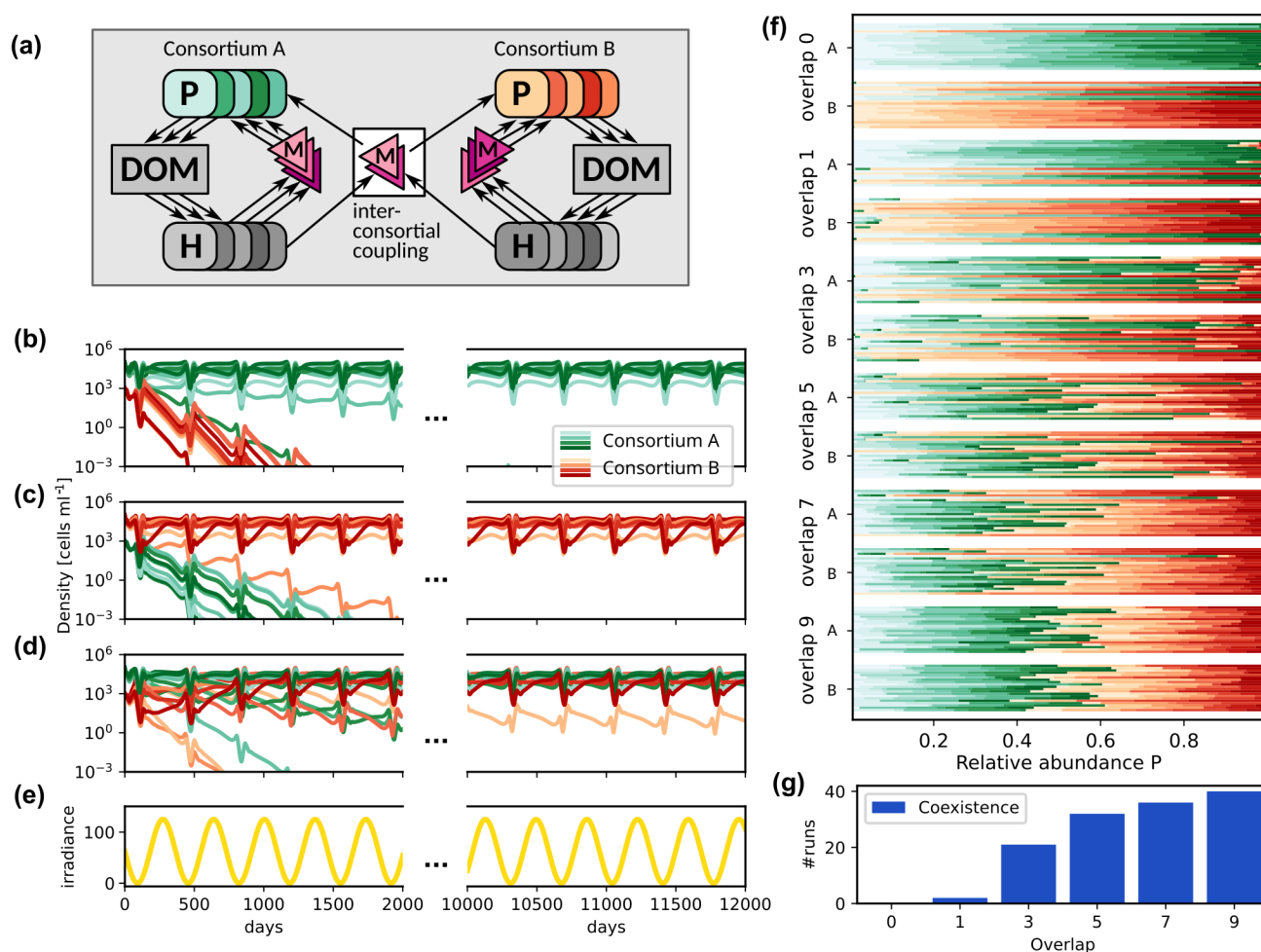
Figure 8. Competition between two consortia for different inter-consortial coupling strength and initial states. (a) Schematic representation of the microbial community consisting of two consortia with inter-consortial coupling by shared metabolites. (b)–(d) Phytoplankton density trajectories; (b) and (c) Priority effects (bi-stability) in case of high connectivity and no coupling: The same interaction network may lead to a competitive exclusion of consortium B by consortium A (b) or *vice versa* (c), depending on which consortium is initially dominant; (d) Dynamics for higher inter-consortial metabolite interactions (overlap 5), leading to coexistence despite initial dominance of consortium A. (e) Periodic variation of the average environmental irradiance; (f) Asymptotic relative abundances for different coupling strengths and initial states. (g) Number of runs displaying coexistence.

these heterotrophs. Although competition between consortium members (for nutrients and DOM) is possible, positive feedback loops within a consortium can be expected to facilitate the growth of its members on average.

For each community, two consortia, A and B, were generated, each consisting of ten phototrophs, ten heterotrophs, ten DOC and ten DON compounds, and ten metabolite types. For the generation, we prescribed the in- and out-degrees of the microbial

370

nodes, i.e., the number of released and consumed compounds, as well as number of produced and effective metabolites (*cf.* Table C4). Then, we randomly connected the different components adhering to these degrees. Further, we allowed for a coupling of the two consortia by defining a number of shared metabolites, which effect both consortia. This number is called "overlap" in the following. Figure 8 (a) shows the community structure schematically.

375   In the following, we assumed an annual cycle of varying average light intensity as shown in Panel (e). Panels (b)–(d) show the time series of simulated phytoplankton population densities for different degrees of inter-consortial coupling and different initial conditions. In Panel (b) and (c), we show two simulations for the same community consisting of two consortia with a single overlapping metabolite. This configuration often leads to priority effects, as exemplified by the depicted dynamics: When the phototrophs of consortium A (green curves) are initialized with higher density than the phototrophs of consortium B [see Panel (b)], consortium A remains dominant over the whole time span of the simulation (approx. 45 years). *Vice versa*,

380   consortium B remains dominant if its phototrophs have higher initial density [Panel (c)].

Panel (d) shows a trajectory in a modified network with higher inter-consortial coupling (overlap 5), where priority effects are not observed, i.e., despite differing initial phototroph densities the trajectories converge to identical periodic orbits after a transient time. In such cases, the 'crosstalk' between consortia prevents their dynamical separation and an equilibrium, where

385   members of both consortia coexist, is attained independently of the initial state.

We explored this effect systematically in different systems. For each of six values of the overlap, we generated 20 communities, each containing two consortia, A and B (20 phototrophs and 20 heterotrophs in total). Each community was initialized twice, with either consortium A or consortium B being dominant, and integrated for 60 years (see Table C4 for a detailed description of parameters). The relative averaged abundance over the last ten years of the simulation is reported for each simu-

390   lation run in Panel (f). Starting from different initial states, where either consortium A or B is dominant, priority effects appear as differences in observed asymptotic distributions for the different initial states.

We categorized all observed regimes either as coexistence, where both consortia contribute more than 10% to the total abundance, or as dominance of either consortium A or B. For low overlap, communities show pronounced priority effects in most cases, where in general the initially dominant consortium remains dominant. For instance, for zero overlap, none of

395   the simulations ended in coexistence [Panel (g)]. However, in 1/8 of the simulations the finally dominating consortium was the initially rare one. For one overlapping metabolite, two of 40 runs led to a coexistence of both consortia. Already for an overlap of three metabolites about 50% of the simulations end in coexistence, and for overlap higher than five (where >30% of metabolites are shared between consortia), species coexistence is the most frequent (>75%) simulation outcome.

5   Conclusions

400   MCoM v1.0 is a versatile, scalable framework for simulating the dynamics of microbial communities consisting of phototrophic and heterotrophic species that includes a wide range of microbial interactions. The processes implemented into MCoM capture essential mechanisms of these interactions, such as nutrient competition, exo-metabolite and DOM production, as well as remineralization. Due to its flexible structure, MCoM allows to explore a range of ecological scenarios, from single-species

experiments (Sher et al., 2011; Christie-Oleza et al., 2017) to complex community interactions (Garcia et al., 2018; Kost et al., 2023). We demonstrated this by simulating simple co-culture experiments, as well as non-linear phenomena such as emergent periodic succession patterns and multi-stability, which are prerequisites for modelling, e.g., ecological tipping points. Aside from aiding mechanistic insights to ecological observations, MCoM may prove useful for the simulation of biotechnological setups as the relevance and the potential of microbial interactions for industrial exploitation becomes increasingly recognized (Ramanan et al., 2016).

MCoM is intentionally kept relatively simple in order to assess fundamental controls of microbial communities and their impact on biogeochemical fluxes. Due to its customizable nature, it offers a robust foundation for future enhancements. Several more detailed process descriptions could be integrated as modular additions, which can be toggled on or off according to the user needs. For instance, incorporating adaptive elemental ratios that vary with environmental conditions (Godwin and Cotner, 2015; Trautwein et al., 2017; Tanioka and Matsumoto, 2020) could further refine its representation of both phytoplankton and heterotrophic processes. Introducing adaptive interaction strategies, as seen in algicidal interactions (Seyedsayamdost et al., 2011; Meyer et al., 2017) and expanding the role of exo-metabolites to influence assimilation rates or other parameters (beyond phytoplankton mortality) would increase the model's versatility. Furthermore, incorporating environmental factors like temperature to modulate growth rates (Coles and Jones, 2000; Bouman et al., 2005) could improve the model's accuracy in scenarios with varying environments. In summary, MCoM provides a versatile platform that is customizable to specific requirements from assessing pairwise interactions to diverse microbial communities. By taking into account the full range of positive and negative interactions, it expands the currently prevailing competition-centred view in biogeochemical modelling.

Code availability. The source code for MCoM v1.0 is published under MIT license and can be downloaded from Zenodo (Lücken et al., 2025). The repository contains the software documentation, instructions on configuration and installation, as well as a test suite. To run MCoM, Julia and Python must be installed (see README.md and requirements.txt for more specific dependencies). For the latest version, please visit https://github.com/bgc-mod/MCoM.

Appendix A: Reference tables

Table A1. Parameters of the MCoM model. All parameters are assumed to be non-negative if not stated otherwise.

Parameter	Description	Source code variable	Unit
$V_{i,N}$	Maximal DIN uptake rates of P_i or H_i	V_NP[i], V_NH[i]	$\mathrm{fmol(N)\,day^{-1}\,cell^{-1}}$
$K_{i,N}$	Half saturation constants for DIN uptake by P_i or H_i	K_NP[i], K_NH[i]	$\mathrm{mM(N)}$
$V_{i,j}$	Maximal uptake rates DOC (resp. DON) compound j uptake by H_i	V_DOCH[j,i], V_DONH[j,i]	$\mathrm{fmol(C)\,day^{-1}\,cell^{-1}}$, $\mathrm{fmol(N)\,day^{-1}\,cell^{-1}}$
$K_{i,j}$	Half saturation constants for DOC (resp. DON) compound j uptake by H_i	K_DOCH[j,i], K_DONH[j,i]	$\mathrm{mM(C)}$, $\mathrm{mM(N)}$
$Y_{i,j}$	Biomass yield coefficients, i.e., fractions of uptake of DOC (resp. DON) compound D_j integrated into biomass of P_i or H_i, $0 \leq Y_{i,j} \leq 1$	Y_DOC[j,i], Y_DON[j,i]	-
χ_i^C	Carbon content per cell of population P_i or H_i	XH_C[i], XP_C[i]	$\mathrm{fmol(C)\,cell^{-1}}$
$r_i^{C:N}, r_{\mathrm{ex},i}^{C:N}$	C:N ratios of populations P_i or H_i, and of N-rich exudates of P_i, $r_i^{C:N} > r_{\mathrm{ex},i}^{C:N}$ for all species.	rCN_P[i], rCN_H[i]	$\mathrm{mol(C)\,mol(N)^{-1}}$
$r_i^{\mathrm{Chl}:C}$	Chlorophyll to carbon ratio for cells of P_i	rChlC[i]	$\mathrm{mol(Chl)\,mol(C)^{-1}}$
$\chi_i^N, \chi_i^{\mathrm{Chl}}$	Nutrient or chlorophyll content per cell ($\chi_i^N = \chi_i^C / r_i^{C:N}$, $\chi_i^{\mathrm{Chl}} = \chi_i^C \cdot r_i^{Chl:C}$)	-	$\mathrm{fmol(N)\,cell^{-1}}$, $\mathrm{fmol(Chl)\,cell^{-1}}$
q_i^{ex}	Maximal fractions of assimilated DOC used for DON exudation of P_i in light limited regime.	q_ex[i]	-
δ_i	Linear loss rates of phytoplankton, heterotrophs, and metabolites	d_P[i], d_H[i], d_M[i]	$\mathrm{day^{-1}}$
$\delta_{q,i}$	Quadratic loss rates of phytoplankton and heterotrophs	d_P2[i]*XP_C[i], d_H2[i]*XH_C[i]	$\mathrm{cell^{-1}\,day^{-1}}$
$a_{i,j}^M$	Interaction rate per unit of metabolite j on growth of phytoplankton population i; can be negative	lambda_i *A_MP[j,i]	$\mathrm{day^{-1}}$
$h_{i,j}$	Half saturation constant for the effect of metabolite j on population i	h_M[j,i]	-
θ_i	Conversion coefficient for determining the amount of metabolite i corresponding to the amount of invested DOC	not included (assumed equal to one)	$\mathrm{mM(C)^{-1}}$
α_i	Slope of the P-I curve of P_i at irradiance $I = 0$. (Effective if variant.use_PI_curve=true)	I_alpha[i]	$\frac{\mathrm{mol(C)\,m^2}}{86400\,\mathrm{mol(Chl)\,\mu mol(Q)}}$
β_i	Photoinhibition coefficient of the P-I curve of P_i. (Effective if variant.use_PI_curve=true)	I_beta[i]	$\frac{\mathrm{mol(C)\,m^2}}{86400\,\mathrm{mol(Chl)\,\mu mol(Q)}}$
$\phi_{s,i}$	Upper limit for the photosynthesis rate of P_i. (Effective if variant.use_PI_curve=true)	I_max[i]	$\mathrm{mol(C)\,mol(Chl)^{-1}\,day^{-1}}$
$R_{j,i}$	Release partition coefficients, $0 \leq R_{j,i} \leq 1$, for $i \in \mathcal{P}$ or $i \in \mathcal{H}$, and $j \in \mathcal{C}$ or $j \in \mathcal{N}$	R_PDOC[i,j], R_PDON[i,j], R_HDOC[i,j], R_HDON[i,j]	-
$\pi_{j,i}$	Production of metabolite j by heterotroph H_i	P_HM[i,j]	-
irrad_min, irrad_max	Range of the average irradiance. (Varies sinusoidally between minimum and maximum in one year.) If variant.use_PI_curve=false, this is interpreted directly as specific photosynthesis rate with unit $\frac{\mu\mathrm{mol\,C}}{\mu\mathrm{mol\,Chl\cdot day}}$.	irrad_min, irrad_max	$\mathrm{\mu mol(Q)\,m^{-2}\,s^{-1}}$

Table A2. Reference table of notations for elemental flows.

Flow	Description	Source	Target	Unit
General population-associated flows ($i \in \mathcal{P}$ or $i \in \mathcal{H}$)				
$f_{N \to i}$	realized inorganic nutrient assimilation into biomass	DIN	P_i or H_i	$\mathrm{fmol(N)\,day^{-1}}$
$f_{N \to i}^{\max}$	maximal inorganic nutrient assimilation into biomass	DIN	P_i or H_i	$\mathrm{fmol(N)\,day^{-1}}$
$f_{i \to \mathrm{DOC}}$	total biomass loss to DOC	P_i or H_i	DOC	$\mathrm{fmol(C)\,day^{-1}}$
$f_{i \to \mathrm{DON}}$	total biomass loss to DON	P_i or H_i	DON	$\mathrm{fmol(N)\,day^{-1}}$
Phytoplankton populations ($i \in \mathcal{P}$)				
$f_{C \to i}$	realized photosynthetic carbon assimilation into biomass	DIC	P_i	$\mathrm{fmol(C)\,day^{-1}}$
$f_{C \to i}^{\max}$	photosynthetic carbon fixation (= maximal assimilation)	DIC	P_i	$\mathrm{fmol(C)\,day^{-1}}$
$f_{C \to \mathrm{DOC}}^{i}$	DOC exudation	DIC	DOC	$\mathrm{fmol(C)\,day^{-1}}$
$f_{N \to \mathrm{DON}}^{i}$	DON exudation	DIN	DON	$\mathrm{fmol(N)\,day^{-1}}$
Heterotroph populations ($i \in \mathcal{H}$)				
$f_{\mathrm{DOC} \to i}, f_{\mathrm{DON} \to i}$	realized total organic carbon, resp. nutrient, assimilation into biomass	DOC, DON	H_i	$\mathrm{fmol(C)\,day^{-1}}, \mathrm{fmol(N)\,day^{-1}}$
$f_{\mathrm{DOC} \to i}^{\max}, f_{\mathrm{DON} \to i}^{\max}$	maximal total organic carbon, resp. nutrient, assimilation into biomass	DOC, DON	H_i	$\mathrm{fmol(C)\,day^{-1}}, \mathrm{fmol(N)\,day^{-1}}$
$f_{j \to i}^{\mathrm{up}}, j \in \mathcal{C} \cup \mathcal{N}$	realized uptake of DOC or DON compound j into biomass	D_j	H_i, and DIC or DIN	$\mathrm{fmol(C)\,day^{-1}}, \mathrm{fmol(N)\,day^{-1}}$
$f_{j \to i}^{\mathrm{up,max}}, j \in \mathcal{C} \cup \mathcal{N}$	maximal uptake of DOC or DON compound j into biomass	D_j	H_i, and DIC or DIN	$\mathrm{fmol(C)\,day^{-1}}, \mathrm{fmol(N)\,day^{-1}}$
$f_{j \to C}^{i}, f_{j \to N}^{i}, j \in \mathcal{C} \cup \mathcal{N}$	remineralization of DOC or DON compound j	D_j	DIC, DIN	$\mathrm{fmol(C)\,day^{-1}}, \mathrm{fmol(N)\,day^{-1}}$
$f_{\mathrm{DON} \to N}^{+}$	surplus nutrient remineralization	DON	DIN	$\mathrm{fmol(N)\,day^{-1}}$
DOC or DON compounds ($j \in \mathcal{C}$ or $j \in \mathcal{N}$)				
$f_{H \to j}$	total heterotroph biomass loss to compound j	H_i	D_j	$\mathrm{fmol(C)\,day^{-1}}, \mathrm{fmol(N)\,day^{-1}}$
$f_{P \to j}$	total phototroph biomass loss to compound j	P_i	D_j	$\mathrm{fmol(C)\,day^{-1}}, \mathrm{fmol(N)\,day^{-1}}$
$f_{C \to j}, f_{N \to j}$	total phototrophic exudation of compound j	DIN, DOC	D_j	$\mathrm{fmol(C)\,day^{-1}}, \mathrm{fmol(N)\,day^{-1}}$
$f_{C \to j}^{i}, f_{N \to j}^{i}, i \in \mathcal{P}$	exudation of compound j by population P_i	DIN, DOC	D_j	$\mathrm{fmol(C)\,day^{-1}}, \mathrm{fmol(N)\,day^{-1}}$
$f_{j \to H}$	total assimilation of compound j into heterotroph biomass	D_j	H_i	$\mathrm{fmol(C)\,day^{-1}}, \mathrm{fmol(N)\,day^{-1}}$
$f_{j \to C}, f_{j \to N}$	total remineralization of compound j	D_j	DIC, DIN	$\mathrm{fmol(C)\,day^{-1}}, \mathrm{fmol(N)\,day^{-1}}$
$f_{i \to j}, i \in \mathcal{P} \cup \mathcal{H}$	biomass loss of population i to compound j	P_i or H_i	D_j	$\mathrm{fmol(C)\,day^{-1}}, \mathrm{fmol(N)\,day^{-1}}$
Nutrient N				
$f_{\mathrm{DON} \to N}$	total remineralization	DON	DIN	$\mathrm{fmol(N)\,day^{-1}}$
$f_{N \to P}, f_{N \to H}$	total assimilation into biomass	DIN	P_i or H_i	$\mathrm{fmol(N)\,day^{-1}}$

Appendix B: Calculation of realized carbon assimilation ($f_{C \to i}$) and DOC exudation rates ($f^i_{C \to \text{DOC}}$)

We use the stoichiometric ratios $r^{C:N}_i$ and $r^{C:N}_{\text{ex},i}$, the maximal assimilation rates $f^{\max}_{C \to i}$ and $f^{\max}_{N \to i}$, and the maximal fraction q^{ex}_i of carbon allocated for exudation to derive the realized assimilation and exudation rates $f_{C \to i}$ and $f^i_{C \to \text{DOC}}$.

430   We assume that carbon is fixated at maximum rate. Since it is fully allocated for assimilation and exudation [Eq. (6)], we have

$$f_{C \to i} = f^{\max}_{C \to i} - f^i_{C \to \text{DOC}}. \tag{B1}$$

Further, the required uptake of N by P_i, that is $f^i_{N \to \text{DON}} + f_{N \to i}$, is related to the total carbon fixation by the stoichiometric composition of assimilation and exudation fluxes [Eqs. (2) and (7)]. Dividing these by the ratios, adding them up, then using

435   Eq. (B1) and some basic algebra gives

$$f_{N \to i} + f^i_{N \to \text{DON}} = \frac{r^{C:N}_{\text{ex},i}}{r^{C:N}_i r^{C:N}_{\text{ex},i}} \cdot f^{\max}_{C \to i} + \frac{r^{C:N}_i - r^{C:N}_{\text{ex},i}}{r^{C:N}_i r^{C:N}_{\text{ex},i}} \cdot f^i_{C \to \text{DOC}}. \tag{B2}$$

Note that the coefficient of $f^i_{C \to \text{DOC}}$ is positive as we assume $r^{C:N}_i > r^{C:N}_{\text{ex},i}$.

     This can be solved for $f^i_{C \to \text{DOC}}$ by maximization under the given constraints

$$f^i_{C \to \text{DOC}} \le q^{\max}_i f^{\max}_{C \to i}, \tag{B3}$$

440   and

$$f_{N \to i} + f^i_{N \to \text{DON}} \le f^{\max}_{N \to i},$$

which, using Eq. (B2), is equivalent to

$$f^i_{C \to \text{DOC}} \le \frac{r^{C:N}_{\text{ex},i}}{r^{C:N}_i - r^{C:N}_{\text{ex},i}} \left(r^{C:N}_i f^{\max}_{N \to i} - f^{\max}_{C \to i} \right). \tag{B4}$$

Hence,

445   $$f^i_{C \to \text{DOC}} = \min \left(q^{\max}_i f^{\max}_{C \to i}, \frac{r^{C:N}_{\text{ex},i}}{r^{C:N}_i - r^{C:N}_{\text{ex},i}} \left(r^{C:N}_i f^{\max}_{N \to i} - f^{\max}_{C \to i} \right) \right).$$

Appendix C: Parameters used in Section 4

Table C1. Parameters for modeling Co-culture experiments of *Synechococcus* and heterotrophic bacteria, see Sec. 4.1.

Parameter	*Synechococcus*	Parameter	*R. Pomeroyi*	*Tropicibacter sp.*
P_0	10^7 cells ml^{-1}	H_0	$5 \cdot 10^5$ cells ml^{-1}	$3 \cdot 10^6$ cells ml^{-1}
χ_C	12.0 fmol(C) cell^{-1}	χ_C	15.0 fmol(C) cell^{-1}	12.0 fmol(C) cell^{-1}
$r_i^{C:N}$	5.2 mol(C) mol(N)$^{-1}$	$r_i^{C:N}$	4.0 mol(C) mol(N)$^{-1}$	4.0 mol(C) mol(N)$^{-1}$
$f_{C \to i}^{\max}$	4.6 fmol(C) day^{-1} cell^{-1} (constant photosynthetic rate)	δ, δ_q	0.1 day^{-1}, 0.45 $(10^6$ cells$)^{-1}$ day^{-1}	0.2 day^{-1}, 0.012 $(10^6$ cells$)^{-1}$ day^{-1}
δ, δ_q	0.28 day^{-1}, 0.0 cell^{-1} day^{-1}	V_N	0.0 fmol(N) cell^{-1} day^{-1}	4.0 fmol(N) cell^{-1} day^{-1}
V_N	1.7 fmol(N) cell^{-1} day^{-1}	K_N	-	0.1 mM(N)
K_N	2.0 mM(N)	V_{DON}	4.0 fmol(N) cell^{-1} day^{-1}	5.2 fmol(N) cell^{-1} day^{-1}
		K_{DON}	0.1 mM(N)	0.1 mM(N)
	Environment	Y_{DON}	0.7	0.95
N_0	8.8 mM(N)	V_{DOC}	6.0 fmol(N) cell^{-1} day^{-1}	12.2 fmol(N) cell^{-1} day^{-1}
Δ	0.0 day^{-1}	K_{DOC}	0.1 mM(C)	0.1 mM(C)
		Y_{DOC}	0.8	0.87
		$R_{lDOC,H}$	0.5	0.99
		$R_{lDOC,P}$	0.9	1.0
		$R_{lDON,H}$	0.9	0.93
		$R_{lDON,P}$	0.9	1.0

Table C2. Parameters for modeling Co-culture experiments of *Prochlorococcus* and heterotrophic bacteria, see Sec. 4.2.

	Prochlorococcus		**Heterotrophs**
P_0	10^6 cells ml^{-1}	H_0	10^4 cells ml^{-1}
χ_C	10.0 fmol(C) cell^{-1}	χ_C	2.0 fmol(C) cell^{-1}
$r_i^{C:N}$	5.0 mol(C) mol(N)$^{-1}$	$r_i^{C:N}$	4.0 mol(C) mol(N)$^{-1}$
$f_{C \to i}^{\max}$	10.0 fmol(C) day^{-1} cell^{-1} (constant photosynthetic rate)	δ, δ_q	0.2 day^{-1}, 0.0 cell^{-1} day^{-1}
δ, δ_q	0.35 day^{-1}, 0.0 cell^{-1} day^{-1}	V_N	1.5 fmol(N) cell^{-1} day^{-1}
V_N	1.25 fmol(N) cell^{-1} day^{-1}	K_N	8.0 mM(N)
K_N	2.4 mM	V_{DON}	3.0 fmol(N) cell^{-1} day^{-1}
		K_{DON}	0.6 mM(N)
	Environment	Y_{DON}	0.6
N_0	800 mM(N)	V_{DOC}	3.0 fmol(N) cell^{-1} day^{-1}
Δ	0.0 day^{-1}	K_{DOC}	0.6 mM(C)
$l\mathrm{DOC}_0$	5.0 mM(C)	Y_{DOC}	0.7
$l\mathrm{DON}_0$	0.05 mM(N)	h_M	$5 \cdot 10^{-7}$
M_0	10^{-9}	π_M	10^{-7}
δ_M	0.3 day^{-1}		
	Rhodobacterales (**HOT5B8**)		*Marinobacter* (**HOT4B5**)
a_M	-0.2	a_M	0.17

Table C3. Parameters used for the cyclic interaction motif, see Sec. 4.3.

Parameter	Phytoplankton	Parameter	Heterotrophs
χ_i^C	$10.0\,\mathrm{fmol(C)\,cell^{-1}}$	χ_i^C	$2.0\,\mathrm{fmol(C)\,cell^{-1}}$
$r_i^{C:N}$	$5.2\,\mathrm{mol(C)\,mol(N)^{-1}}$	$r_i^{C:N}$	$4.0\,\mathrm{mol(C)\,mol(N)^{-1}}$
$\delta_i, \delta_{q,i}$	$0.2\,\mathrm{day^{-1}}, 0.2\,(10^6\,\mathrm{cells})^{-1}\,\mathrm{day^{-1}}$	$\delta_i, \delta_{q,i}$	$0.1\,\mathrm{day^{-1}}, 0.02\,(10^6\,\mathrm{cells})^{-1}\,\mathrm{day^{-1}}$
$h_{i,j}$	10^{-4}	$\pi_{j,i}$	10^{-5}
$a_{i,j}^M$	0.0 or -1.0	**Nutrient uptake**	
$V_{i,N}$	$1.0\,\mathrm{fmol(N)\,cell^{-1}\,day^{-1}}$	$V_{i,N}$	$1.5\,\mathrm{fmol(N)\,cell^{-1}\,day^{-1}}$
$K_{i,N}$	$2.0\,\mathrm{mM(N)}$	$K_{i,N}$	$8.0\,\mathrm{mM(N)}$
$\phi_{s,i}$	$5.0\,\mathrm{mol(C)\,mol(Chl)^{-1}\,day^{-1}}$	**DON uptake**	
α_i	$0.08\,\frac{\mathrm{mol(C)\,m^2}}{86400\,\mathrm{mol(Chl)\,\mu mol(Q)}}$	$V_{i,j}$	$3.0\,\mathrm{fmol(N)\,cell^{-1}\,day^{-1}}$
β_i	$0.003\,\frac{\mathrm{mol(C)\,m^2}}{86400\,\mathrm{mol(Chl)\,\mu mol(Q)}}$	$K_{i,j}$	$1.0\,\mathrm{mM(N)}$
		$Y_{i,j}$	0.5
Environment		**DOC uptake**	
Δ	$0.1\,\mathrm{day^{-1}}$	$V_{i,j}$	$4.0\,\mathrm{fmol(N)\,cell^{-1}\,day^{-1}}$
δ_M	$0.1\,\mathrm{day^{-1}}$	$K_{i,j}$	$1.0\,\mathrm{mM(C)}$
N_{ext}	$5.0\,\mathrm{mM(N)}$	$Y_{i,j}$	0.5
I	$10.0\,\mathrm{\mu mol(Q)\,m^{-2}\,day^{-1}}$		

Table C4. Parameters used for the simulation of two competing consortia, see Sec. 4.4

Parameter	Phytoplankton	Parameter	Heterotrophs
$P_i(0)$	10^8, resp. 10^6, cells ml^{-1}	$H_i(0)$	10^5–10^7 cells ml^{-1}
χ_i^C	10.0 fmol(C) cell^{-1}	χ_i^C	2.0 fmol(C) cell^{-1}
$r_i^{C:N}$	5.2 mol(C) mol(N)$^{-1}$	$r_i^{C:N}$	4.0 mol(C) mol(N)$^{-1}$
$\delta_i, \delta_{q,i}$	0.1 day^{-1}, $1.0\,(10^6$ cells$)^{-1}$ day^{-1}	$\delta_i, \delta_{q,i}$	0.1 day^{-1}, $0.02\,(10^6$ cells$)^{-1}$ day^{-1}
$h_{i,j}$	10^{-4}	$\pi_{j,i}$	10^{-5}
$a_{i,j}^M$	0.0 or -0.1	**Nutrient uptake**	
$V_{i,N}$	1.0 fmol(N) cell^{-1} day^{-1}	$V_{i,N}$	1.5 fmol(N) cell^{-1} day^{-1}
$K_{i,N}$	2.0 mM(N)	$K_{i,N}$	8.0 mM(N)
$\phi_{s,i}$	3.0–5.0 mol(C) mol(Chl)$^{-1}$ day^{-1}	**DON uptake**	
α_i	0.05–$0.3\ \frac{\text{mol(C)\,m}^2}{86400\,\text{mol(Chl)\,µmol(Q)}}$	$V_{i,j}$	3.0 fmol(N) cell^{-1} day^{-1}
β_i	0.003–$0.08\ \frac{\text{mol(C)\,m}^2}{86400\,\text{mol(Chl)\,µmol(Q)}}$	$K_{i,j}$	1.0 mM(N)
		$Y_{i,j}$	0.5
Environment		**DOC uptake**	
Δ	0.1 day^{-1}	$V_{i,j}$	4.0 fmol(N) cell^{-1} day^{-1}
N_0	8.8 mM(N)	$K_{i,j}$	1.0 mM(C)
δ_M	0.1 day^{-1}	$Y_{i,j}$	0.5
N_ext	5.0 mM(N)		
I_min	0.0 µmol(Q) m^{-2} day^{-1}	**Connectivity**	
I_max	125.0 µmol(Q) m^{-2} day^{-1}	exPDOC	4
		exPDON	4
System dimensions		exHDOC	4
dims.P	20	exHDON	4
dims.H	20	upDOCH	3
dims.DOC	20	upDONH	3
dims.DON	20	prodHM	2
dims.M	10–20 (overlap-depd.)	effsMP	4

References

Amin, S. A., Hmelo, L. R., van Tol, H. M., Durham, B. P., Carlson, L. T., Heal, K. R., Morales, R. L., Berthiaume, C. T., Parker, M. S., Djunaedi, B., Ingalls, A. E., Parsek, M. R., Moran, M. A., and Armbrust, E. V.: Interaction and signalling between a cosmopolitan phytoplankton and associated bacteria, Nature, 522, 98–101, https://doi.org/10.1038/nature14488, 2015.

Becker, J. W., Berube, P. M., Follett, C. L., Waterbury, J. B., Chisholm, S. W., DeLong, E. F., and Repeta, D. J.: Closely related phytoplankton species produce similar suites of dissolved organic matter, Frontiers in Microbiology, 5, https://doi.org/10.3389/fmicb.2014.00111, 2014.

Bouman, H., Platt, T., Sathyendranath, S., and Stuart, V.: Dependence of light-saturated photosynthesis on temperature and community structure, Deep Sea Research Part I: Oceanographic Research Papers, 52, 1284–1299, https://doi.org/10.1016/j.dsr.2005.01.008, 2005.

Buchan, A., LeCleir, G. R., Gulvik, C. A., and González, J. M.: Master Recyclers: Features and Functions of Bacteria Associated with Phytoplankton Blooms, Nature Reviews Microbiology, 12, 686–698, https://doi.org/10.1038/nrmicro3326, 2014.

Butcher, J. C., ed.: Numerical Methods for Ordinary Differential Equations, Wiley, Chichester, ISBN 978-0-471-96758-3 978-0-470-86827-0, https://doi.org/10.1002/0470868279, 2005.

Christie-Oleza, J. A., Sousoni, D., Lloyd, M., Armengaud, J., and Scanlan, D. J.: Nutrient Recycling Facilitates Long-Term Stability of Marine Microbial Phototroph–Heterotroph Interactions, Nature Microbiology, 2, 17 100, https://doi.org/10.1038/nmicrobiol.2017.100, 2017.

Cirri, E. and Pohnert, G.: Algae-bacteria interactions that balance the planktonic microbiome, New Phytologist, 223, 100–106, https://doi.org/10.1111/nph.15765, 2019.

Coles, J. F. and Jones, R. C.: Effect of temperature on photosynthesis-light response and growth of four phytoplankton species isolated from a tidal freshwater river, Journal of Phycology, 36, 7–16, https://doi.org/10.1046/j.1529-8817.2000.98219.x, 2000.

Coyne, K. J., Wang, Y., and Johnson, G.: Algicidal Bacteria: A Review of Current Knowledge and Applications to Control Harmful Algal Blooms, Frontiers in Microbiology, 13, https://doi.org/10.3389/fmicb.2022.871177, 2022.

De Mazancourt, C. and Schwartz, M. W.: A resource ratio theory of cooperation, Ecology Letters, 13, 349–359, https://doi.org/10.1111/j.1461-0248.2009.01431.x, 2010.

Elovaara, S., Eronen-Rasimus, E., Asmala, E., Tamelander, T., and Kaartokallio, H.: Contrasting patterns of carbon cycling and dissolved organic matter processing in two phytoplankton–bacteria communities, Biogeosciences, 18, 6589–6616, https://doi.org/10.5194/bg-18-6589-2021, 2021.

Friedrichs, M. A. M., Dusenberry, J. A., Anderson, L. A., Armstrong, R. A., Chai, F., Christian, J. R., Doney, S. C., Dunne, J., Fujii, M., Hood, R., McGillicuddy, D. J., Moore, J. K., Schartau, M., Spitz, Y. H., and Wiggert, J. D.: Assessment of skill and portability in regional marine biogeochemical models: Role of multiple planktonic groups, Journal of Geophysical Research: Oceans, 112, https://doi.org/10.1029/2006jc003852, 2007.

Garcia, S. L., Buck, M., Hamilton, J. J., Wurzbacher, C., Grossart, H.-P., McMahon, K. D., and Eiler, A.: Model Communities Hint at Promiscuous Metabolic Linkages between Ubiquitous Free-Living Freshwater Bacteria, mSphere, 3, https://doi.org/10.1128/msphere.00202-18, 2018.

Godwin, C. M. and Cotner, J. B.: Stoichiometric flexibility in diverse aquatic heterotrophic bacteria is coupled to differences in cellular phosphorus quotas, Frontiers in Microbiology, 6, https://doi.org/10.3389/fmicb.2015.00159, 2015.

Kazamia, E., Sutak, R., Paz-Yepes, J., Dorrell, R. G., Vieira, F. R. J., Mach, J., Morrissey, J., Leon, S., Lam, F., Pelletier, E., et al.: Endocytosis-mediated siderophore uptake as a strategy for Fe acquisition in diatoms, Science Advances, 4, eaar4536, 2018.

Koffel, T., Daufresne, T., and Klausmeier, C. A.: From Competition to Facilitation and Mutualism: A General Theory of the Niche, Ecological Monographs, 91, https://doi.org/10.1002/ecm.1458, 2021.

Kost, C., Patil, K. R., Friedman, J., Garcia, S. L., and Ralser, M.: Metabolic exchanges are ubiquitous in natural microbial communities, Nature Microbiology, 8, 2244–2252, https://doi.org/10.1038/s41564-023-01511-x, 2023.

Lücken, L., Follows, M. J., Bragg, J. G., and Lennartz, S. T.: MCoM v1.0.0, https://doi.org/10.5281/ZENODO.15433581, 2025.

Maldonado, M. T. and Price, N. M.: Utilization of iron bound to strong organic ligands by plankton communities in the subarctic Pacific Ocean, Deep Sea Research Part II: Topical Studies in Oceanography, 46, 2447–2473, 1999.

Meyer, N., Bigalke, A., Kaulfuß, A., and Pohnert, G.: Strategies and ecological roles of algicidal bacteria, FEMS Microbiology Reviews, 41, 880–899, https://doi.org/10.1093/femsre/fux029, 2017.

Morris, J. J., Rose, A. L., and Lu, Z.: Reactive oxygen species in the world ocean and their impacts on marine ecosystems, Redox Biology, 52, 102 285, https://doi.org/10.1016/j.redox.2022.102285, 2022.

Myklestad, S. M.: Dissolved Organic Carbon from Phytoplankton, vol. 5D, pp. 111–148, Springer-Verlag, Berlin/Heidelberg, ISBN 3540660208, https://doi.org/10.1007/10683826_5, 2000.

Mühlenbruch, M., Grossart, H., Eigemann, F., and Voss, M.: Mini-review: Phytoplankton-derived polysaccharides in the marine environment and their interactions with heterotrophic bacteria, Environmental Microbiology, 20, 2671–2685, https://doi.org/10.1111/1462-2920.14302, 2018.

Platt, T., Gallegos, C. L., and Harrison, W. G.: Photoinhibition of Photosynthesis in Natural Assemblages of Marine Phytoplankton, Journal of Marine Research, 38, 1980.

Ramanan, R., Kim, B.-H., Cho, D.-H., Oh, H.-M., and Kim, H.-S.: Algae–bacteria interactions: evolution, ecology and emerging applications, Biotechnology advances, 34, 14–29, 2016.

Saad, E. M., Longo, A. F., Chambers, L. R., Huang, R., Benitez-Nelson, C., Dyhrman, S. T., Diaz, J. M., Tang, Y., and Ingall, E. D.: Understanding marine dissolved organic matter production: Compositional insights from axenic cultures of Thalassiosira pseudonana, Limnology and Oceanography, 61, 2222–2233, https://doi.org/10.1002/lno.10367, 2016.

Sarmento, H., Romera-Castillo, C., Lindh, M., Pinhassi, J., Sala, M. M., Gasol, J. M., Marrase, C., and Taylor, G. T.: Phytoplankton species-specific release of dissolved free amino acids and their selective consumption by bacteria, Limnology and Oceanography, 58, 1123–1135, https://doi.org/10.4319/lo.2013.58.3.1123, 2013.

Seyedsayamdost, M. R., Case, R. J., Kolter, R., and Clardy, J.: The Jekyll-and-Hyde Chemistry of Phaeobacter Gallaeciensis, Nature Chemistry, 3, 331, 2011.

Seymour, J. R., Amin, S. A., Raina, J.-B., and Stocker, R.: Zooming in on the phycosphere: the ecological interface for phytoplankton–bacteria relationships, Nature microbiology, 2, 1–12, 2017.

Sher, D., Thompson, J. W., Kashtan, N., Croal, L., and Chisholm, S. W.: Response of *Prochlorococcus* Ecotypes to Co-Culture with Diverse Marine Bacteria, The ISME Journal, 5, 1125–1132, https://doi.org/10.1038/ismej.2011.1, 2011.

Sultana, S., Bruns, S., Wilkes, H., Simon, M., and Wienhausen, G.: Vitamin B12 Is Not Shared by All Marine Prototrophic Bacteria with Their Environment, The ISME Journal, 17, 836–845, https://doi.org/10.1038/s41396-023-01391-3, 2023.

Séférian, R., Bopp, L., Gehlen, M., Orr, J. C., Ethé, C., Cadule, P., Aumont, O., Salas y Mélia, D., Voldoire, A., and Madec, G.: Skill assessment of three earth system models with common marine biogeochemistry, Climate Dynamics, 40, 2549–2573, https://doi.org/10.1007/s00382-012-1362-8, 2012.

Tagliabue, A.: 'Oceans Are Hugely Complex': Modelling Marine Microbes Is Key to Climate Forecasts, Nature, 623, 250–252,
530   https://doi.org/10.1038/d41586-023-03425-4, 2023.

Tanioka, T. and Matsumoto, K.: A meta-analysis on environmental drivers of marine phytoplankton C:N:P, Biogeosciences, 17, 2939–2954,
         https://doi.org/10.5194/bg-17-2939-2020, 2020.

Teeling, H., Fuchs, B. M., Becher, D., Klockow, C., Gardebrecht, A., Bennke, C. M., Kassabgy, M., Huang, S., Mann, A. J., Waldmann,
         J., Weber, M., Klindworth, A., Otto, A., Lange, J., Bernhardt, J., Reinsch, C., Hecker, M., Peplies, J., Bockelmann, F. D., Callies, U.,
535   Gerdts, G., Wichels, A., Wiltshire, K. H., Glöckner, F. O., Schweder, T., and Amann, R.: Substrate-Controlled Succession of Marine
         Bacterioplankton Populations Induced by a Phytoplankton Bloom, Science, 336, 608–611, https://doi.org/10.1126/science.1218344, 2012.

Thornton, D. C.: Dissolved organic matter (DOM) release by phytoplankton in the contemporary and future ocean, European Journal of
         Phycology, 49, 20–46, https://doi.org/10.1080/09670262.2013.875596, 2014.

Trautwein, K., Feenders, C., Hulsch, R., Ruppersberg, H. S., Strijkstra, A., Kant, M., Vagts, J., Wünsch, D., Michalke, B., Maczka, M.,
540   Schulz, S., Hillebrand, H., Blasius, B., and Rabus, R.: Non-Redfield, Nutrient Synergy and Flexible Internal Elemental Stoichiometry in
         a Marine Bacterium, FEMS Microbiology Ecology, 93, https://doi.org/10.1093/femsec/fix059, 2017.